



Transport measurements in single-grain GdBCO+Ag bulk superconductors processed by infiltration growth

Pablo Cayado^{1,2} · Devendra K. Namburi^{3,4} · Manuela Erbe¹ · Jens Hänisch¹ · David A. Cardwell³ · John H. Durrell³ · Bernhard Holzapfel¹

Received: 9 November 2022 / Accepted: 7 January 2023
© The Author(s) 2023

Abstract

Transport measurements performed on a cross-sectional slice prepared from a bulk $\text{GdBa}_2\text{Cu}_3\text{O}_{7-x}$ -Ag single-grain superconductor of 25 mm in diameter are described and the results presented. The sample, which was fabricated via the buffer-assisted top-seeded infiltration growth process, was capable of trapping a maximum magnetic field of ~ 1 T at 77 K. Transport measurements on superconducting, bulk single-grain RE-Ba-Cu-O [(RE)BCO] samples are generally very challenging due to their large critical current densities and poor mechanical properties. We present a straightforward and reliable approach to prepare reproducibly specimens from the parent single grain and results of transport property measurements on these samples in a commercial Physical Property Measurement System (PPMS). Critical current densities determined via magnetic and transport measurements are compared and discussed.

Keywords GdBCO · Bulk superconductor · Infiltration and growth technique · Transport measurements · Microstructure · Magnetic properties

1 Introduction

Significant progress has been made in the melt processing of RE-Ba-Cu-O [(RE)BCO, RE = rare earth] bulk high-temperature superconductors over the last three decades, and in particular over the last ten years. Developments in processing have led to pathways for deploying these technologically

important materials in several potential and practical applications including trapped-field magnets, magnetic levitation devices, superconducting motors and generators, flywheels, portable magnetic resonance imaging (MRI) and large-gradient magnetic separation systems [1–5].

Single grain (RE)BCO bulk superconductors with a microstructure engineered for optimum flux pinning exhibit large critical current densities (J_c). These samples (typically ~ 25 mm in diameter) can trap magnetic fields of ~ 0.8 – 1 T at 77 K and ~ 6 – 8 T at 30 K at the sample surface [2, 3, 5] when fully magnetised. Information on J_c in bulk, single grain (RE)BCO superconductors is often obtained via magnetometry, which relies fundamentally on several computational assumptions [6, 7]. This usually involves a combination of a SQUID magnetometer within a cryomagnet, such as a Physical Property Measurement System (PPMS), to determine the magnetic hysteresis (M – H) loops from which the (magnetic) critical current densities (J_c^{mag}) are determined using the extended Bean critical-state model [6].

Critical currents in these materials are measured most commonly via magnetic measurements given the difficulty of preparing specimens for transport measurements on these brittle, ceramic-like materials. For example, the typical

Pablo Cayado and Devendra K. Namburi contributed equally to this work.

✉ Pablo Cayado
pablo.cayado@unige.ch

✉ Devendra K. Namburi
ndevendra@gmail.com

¹ Institute for Technical Physics (ITEP), Karlsruhe Institute of Technology (KIT), Hermann-von-Helmholtz-Platz 1, 76344 Eggenstein-Leopoldshafen, Germany

² Department of Quantum Matter Physics (DQMP), University of Geneva, Quai Ernest-Ansermet 24, 1211 Geneva, Switzerland

³ Department of Engineering, University of Cambridge, Cambridge CB2 1PZ, UK

⁴ Electronic and Nanoscale Engineering, University of Glasgow, Glasgow G11 6EW, UK

J_c^{mag} for YBCO is 40 kA/cm^2 at 77 K, in zero-field [8], which means that the specimen's cross-section for measurement of the critical transport current needs to be smaller than $0.5 \text{ mm} \times 0.5 \text{ mm}$ (cross-sectional area: 0.25 mm^2) for a 100 A current source in a transport measurement. It is extremely challenging to prepare specimens of these dimensions given the brittle nature of (RE)BCO materials. In addition, these bulks usually contain numerous cracks, secondary phases and inclusions that can be of this characteristic dimension and therefore potentially block any transport current completely. Despite these challenges, transport measurements have indeed been reported on (RE)BCO bulk materials by Rush et al. on a GdBCO single-grain bulk [7] and by Kikegawa et al. on a mixed rare earth (Nd-Eu-Gd) BCO sample [9]. Both of these samples were produced via the top-seeded melt growth (TSMG) technique, which typically and unavoidably produces a sample microstructure that contains many pores and cracks due to limitations of the processing technique. A typical cross-section of a YBCO sample obtained via TSMG is shown in Fig. 1. A porosity of $\sim 16\text{--}20\%$ is commonly observed in these samples [2, 10–12].

More recently, infiltration and growth [12–15] has emerged as a new potential processing approach and is enabling the reliable fabrication of (RE)BCO bulk

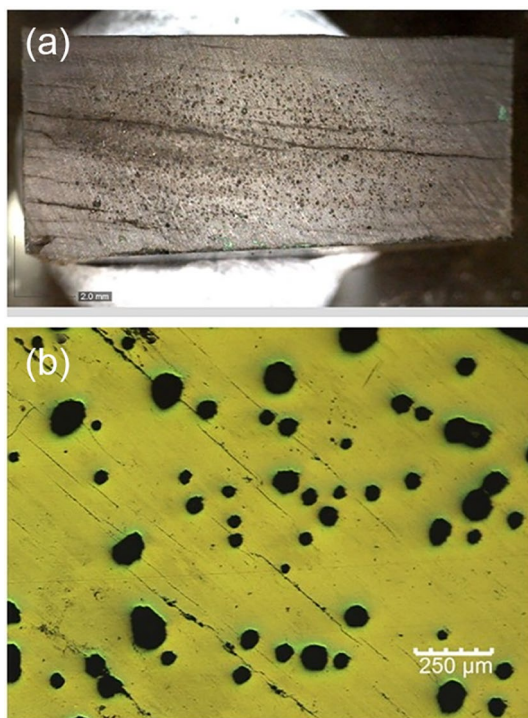


Fig. 1 **a** Cross-section of a YBCO sample fabricated via top-seeded melt growth (TSMG). A higher-resolution optical micrograph is shown in **(b)**. The presence of pores (20–250 μm) and cracks can be seen in both parts of the figure

superconductors with improved microstructures and associated enhanced superconducting and mechanical properties. This motivated us to investigate whether thin, long slices of (RE)BCO bulk superconductors fabricated by infiltration growth can be prepared successfully for transport measurements. In the present work, transport measurements on a GdBCO+Ag sample fabricated via buffer-assisted top-seeded infiltration and growth (BA-TSIG) are described and their results presented and discussed for the first time.

2 Experimental

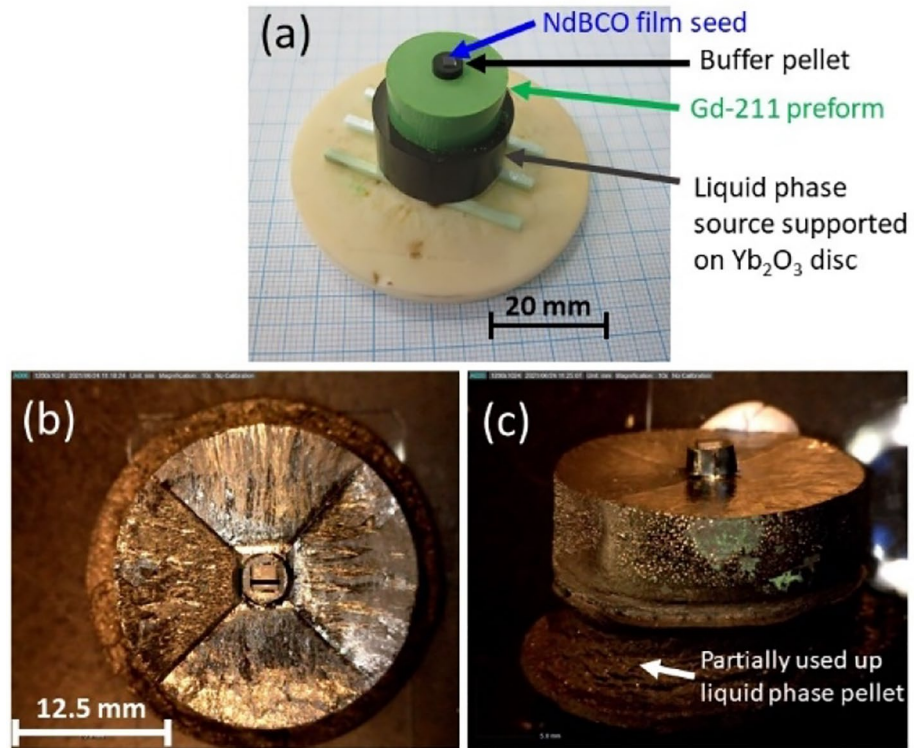
2.1 GdBCO+Ag bulk sample preparation

To produce a single-grain GdBCO sample via TSIG, precursor powders of $\text{Gd}_2\text{BaCuO}_5$ (Gd-211), $\text{Ba}_3\text{Cu}_5\text{O}_8$ (each 99.9% purity, particle size 1–3 μm , Toshima Manufacturing), CeO_2 , BaO_2 , Ag_2O (each > 95% purity, Sigma Aldrich), and Yb_2O_3 (> 98% purity, American Elements) were mixed in the appropriate ratios. To prepare the preform and liquid source pellets, the precursor powders were mixed separately in an automixer for 2 h. A mixture of Gd-211, Ag_2O , BaO_2 , and CeO_2 in a composition of Gd-211 + 10 wt.% Ag_2O + 2 wt.% BaO_2 + 1 wt.% CeO_2 was used for the preform pellet. The composition of the Yb-based liquid phase was $\text{Yb}_2\text{O}_3:\text{CuO}:\text{BaCuO}_2 = 1:10:6$ by molar ratio [16]. The preform pellets were prepared by compacting the respective mixed powders in steel dies using a uniaxial press. The resulting preform pellet ($\sim 25 \text{ mm}$ in diameter) was placed on top of the liquid phase reservoir pellet ($\sim 31 \text{ mm}$ in diameter), and the entire assembly was supported by an Yb_2O_3 substrate to prevent outflow of the liquid phase during the heat treatment. A buffer pellet composed of 75% Gd-123 + 25% Gd-211 capped with a seed crystal (a Nd-based thin-film seed crystal, Ceraco Ceramic Coating GmbH) was placed on top of the sample pellet. The entire arrangement, Fig. 2a, was heat-treated in air in a box furnace for obtaining single-grain growth. The top- and side-views of the as-processed single-grain GdBCO+Ag sample are shown in Fig. 2b, c, respectively. This sample was oxygenated subsequently in a tube furnace at 400 $^\circ\text{C}$ for 200 h to complete the tetragonal-to-orthorhombic crystal structure transformation to produce a superconducting single-grain.

2.2 Magnetic property characterization

The top and bottom surfaces of the sample were polished prior to magnetic measurements and oriented such that the external magnetic field (B_a) was applied parallel to the c -axis of the sample for field-cooled magnetization (FCM). The sample was then cooled to 77 K in an applied magnetic field of 1.3 T, and after achieving thermal equilibrium, the

Fig. 2 a Sample assembly used to fabricate a GdBCO+Ag single-grain via the buffer-aided TSIG technique. The Gd-211 preform (containing added Ag_2O , BaO_2 and CeO_2) was compacted into a pellet of 25 mm diameter. This was supported by a liquid phase reservoir pellet. NdBCO film seed and a buffer pellet are placed on top of the Gd-211 preform pellet to aid heterogeneous nucleation and growth of a single-grain. The top and side-views of the heat-treated sample are shown in (b) and (c), respectively



applied magnetic field was removed and the trapped magnetic field profile of the sample measured with a rotational Hall-probe scanning facility comprised of 19 Hall sensors mounted on a measurement rig.

The magnetic properties of local regions ($a \times b \times c \sim 2 \times 1.5 \times 1 \text{ mm}^3$) of the sample were measured subsequently using a Magnetic Property Measurement System magnetometer (MPMS, Quantum Design). The external magnetic field (B_a) was applied parallel to the crystallographic c -axis at each position in the sample. The magnetic moment was measured as a function of temperature and field to determine T_c and $J_c(B)$. Self-field J_c (J_c^{sf}) at 77 K was measured inductively with a Cryoscan (*Theva*, $50 \mu\text{V}$ criterion). The T_c (determined as T_{c90} , i.e., the temperature at which the resistance is 90% of the value just above the transition), ΔT_c ($T_{c90} - T_{c10}$) and $J_c(B)$ ($1 \mu\text{V cm}^{-1}$ criterion of transport J_c) were measured with a 9 T *Quantum Design* PPMS.

2.3 Sample preparation for transport measurements

To measure the transport properties, thin discs of $\sim 1 \text{ mm}$ thickness were cut from the original bulk single-grain sample with a diamond saw (Isomet). Such thicknesses are still not suitable for transport measurements, so it was necessary to reduce them further. This was achieved by gluing each slice on a substrate ($10 \times 10 \text{ mm}^2$ LaAlO_3 single-crystal) using Ag paint to enable

mechanical polishing. This process is delicate and was hence carried out very carefully and with high accuracy to avoid any breakage of the sample. This involved installing the specimen in an Ar-ion cross-section polisher (IB-19500CP, *JEOL*) where the thickness of the samples was reduced to $25 \mu\text{m}$, which was more practical for measuring the superconducting transport properties with the current source available. Reducing the thickness further would increase the risk of sample breakage considerably, so all transport measurements were performed on a single slice of $25 \mu\text{m}$ thickness.

Photolithography and wet-chemical etching were employed to prepare individual tracks for the transport measurement once the appropriate track thickness had been achieved. To avoid selection bias as much as possible, the track was positioned at random, although slight differences in defect density cannot be excluded completely. The dimensions of the tracks were determined by a LEO 1530 scanning electron microscope (SEM, Zeiss) with field emission gun. The average width of the track was $\sim 110 \mu\text{m}$, as can be seen in Fig. 3. In summary, the measured tracks were $25 \mu\text{m}$ thick, $110 \mu\text{m}$ wide and 1 mm long.

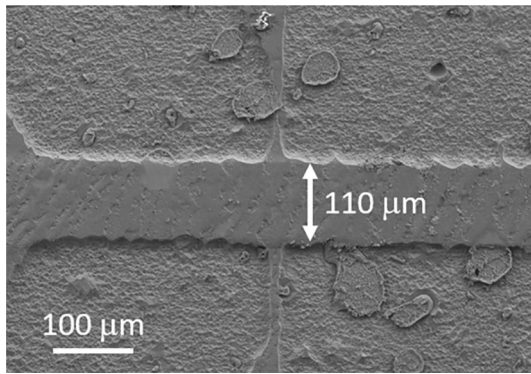


Fig. 3 Scanning electron micrograph of a track on the ion-milled slice of GdBCO+Ag that was prepared for the transport current measurements. The width of the track is $\sim 110 \mu\text{m}$

3 Results and discussion

3.1 Field trapping ability

The trapped magnetic field at 77 K obtained at a distance of 1.5 mm from the surface of the sample is shown in Fig. 4. The sample of ~ 25 mm diameter is clearly a single grain (exhibiting a single field cone) and exhibits a peak trapped magnetic field of ~ 0.87 T at a Hall sensor to sample separation of 1.5 mm, which corresponds to ~ 1 T at the sample surface [17].

3.2 Magnetisation performance

Magnetic moment (and hence magnetization) as a function of temperature and applied field were measured in separate experiments. A critical temperature $T_c \sim 93.5$ K was

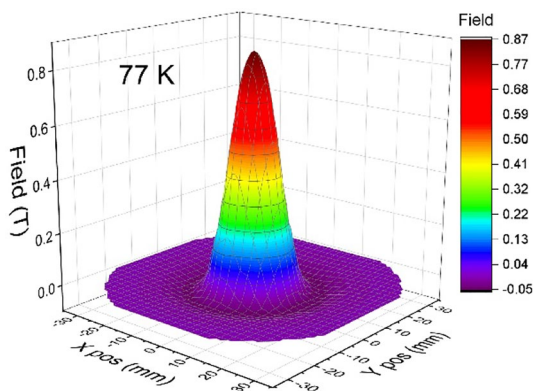


Fig. 4 Trapped field profile measured at 77 K, at a separation of 1.5 mm from the surface of the GdBCO+Ag sample (#1232). The sample trapped a magnetic field of 1 T at its surface and 0.87 T at height of 1.5 mm from the surface of the sample

observed, Fig. 5a, and the superconducting to normal transition occurred within a temperature range of 0.5–1 K (i.e. the transition width). $J_c(B)$ values were estimated in the temperature range of 50–85 K from the width of the magnetic hysteresis (M–H) loops following the extended Bean critical-state model [6], Fig. 5b. The self-field magnetization $J_c, J_{c,\text{mag}}^{\text{sf}}$, at 77 K is ~ 51 kA/cm². The sample exhibited a magnetically measured irreversibility field of ~ 6 T at 77 K.

3.3 Transport measurements

The GdBCO + Ag specimen shown in Fig. 3 exhibits a transport T_c of 93.7 K, as illustrated in the inset of Fig. 6a. This value is very similar to that determined by magnetic measurement (93.5 K) and is also close to that reported for GdBCO thin films prepared at Karlsruhe Institute of Technology (KIT) [18]. Figure 6a shows the temperature dependence of the electrical resistance of the single-grain specimen at several magnetic fields. The data for the irreversibility field (B_{irr}) were extracted from this figure and the resulting irreversibility line (IRL) is shown in Fig. 6b,

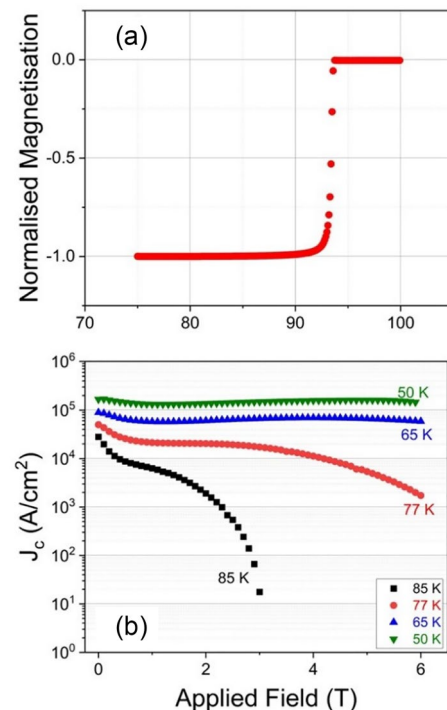


Fig. 5 **a** Magnetisation as a function of temperature measured in a GdBCO+Ag single-grain slice. A critical temperature of ~ 93.5 K with a transition width < 1 K was observed. **b** Magnetic field dependence of the magnetization critical current density J_c of the same sample at several temperatures

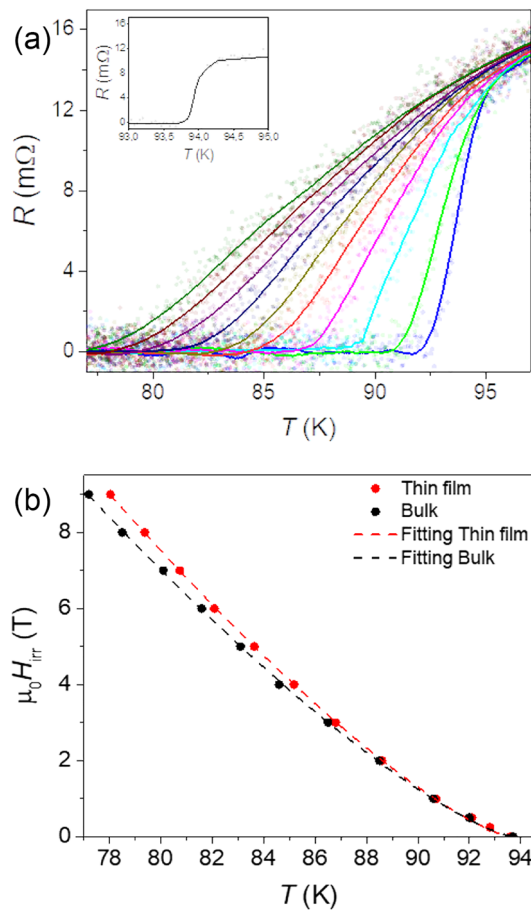


Fig. 6 Temperature dependence of electrical resistance R measured for the IG-processed GdBCO+Ag prepared specimen (a, inset) in the absence of an applied magnetic field and (a) under different magnetic fields in the range 1–9 T (B||c-axis, step size 1 T) and 0.5 T. The irreversibility line (IRL) of the sample (black circles and dashed line) in (b) is compared to a similar curve for a standard, pristine GdBCO film (red circles and red dashed line) [18, 19]. The dashed lines are a fit of the data to expression (1)

together with the IRL of a standard, pristine GdBCO thin film of the same type as the reference sample in [18, 19]. The IRLs of both films were fitted with the following expression:

$$B_{irr}(T) = B_0 \left(1 - \frac{T}{T_c^0} \right)^n \quad (1)$$

where T_c^0 is the irreversibility temperature at zero applied field or simply the T_c of the sample, and B_0 and n are fitting parameters. In the case of the thin film, the values of both fitting parameters are $B_0 = 95.65 \pm 2$ T and $n = 1.318 \pm 0.009$ whereas for the bulk sample they are $B_0 = 89 \pm 2$ T and $n = 1.32 \pm 0.01$. It is clear from these values that both samples behave very similarly with the exponent being close to the expected value of $4/3$ for a glass-liquid transition.

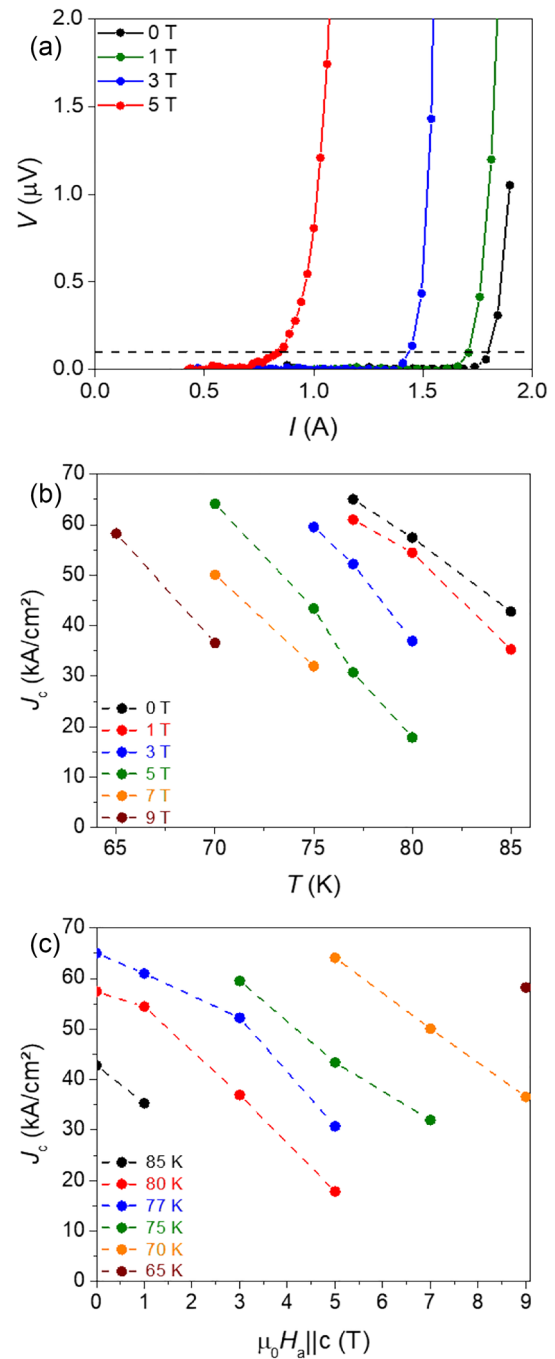


Fig. 7 a Examples of the V – I curves measured on the sliced IG-processed GdBCO+Ag single-grain used for obtaining the J_c values. J_c is shown as a function of applied field (in the range 0–9 T) and temperature (65–85 K) in (b) and (c), respectively. The dashed lines are guides for the eye

The slightly larger absolute values of B_0 observed for the thin film are possibly related to a more complex or optimal microstructure of the sample.

The V – I curves, from which the J_c values were calculated using a criterion of $1 \mu V cm^{-1}$, show the typical power-law

form, Fig. 7a. Figures 7b, c show the temperature and field dependence of J_c for several magnetic fields and temperatures, respectively. Although only a limited number of data points could be obtained in these experiments, the well-known decrease of J_c with T and B is obvious in Figs. 7b, c. It was not possible to measure J_c below 65 K because of the current limit of the PPMS (2 A), so, as a result, self-field values below 77 K were not determined in this study. The transport J_c^{sf} at 77 K is ~ 65 kA/cm². This value should be similar to that measured for the same sample prior to the fabrication of the track. To check if this is the case, the bulk specimen with a thickness of 25 μm was measured by Cryoscan and exhibited a $J_c^{\text{sf}} \sim 68$ kA/cm², which is very similar to that obtained from the transport measurements for the bridge specimen. Significantly, these two values are $\sim 20\%$ larger than that measured by MPMS, which was ~ 51 kA/cm². Although both values are not the same, they are not extremely different. This difference is inherent when the J_c values obtained by magnetometry or by transport are compared in general, which is a well-known phenomenon. This moderate variation in J_c as measured via these two approaches can be understood further by the typical change of the electrical field criterion between the magnetometry and transport techniques [20]. Finally, it should be emphasised that, even though the transport measurements provide a direct measurement of J_c , their accuracy depends critically on the geometrical accuracy of the dimensions of the bridge. It is apparent in Fig. 3 that the edges of both sides of the bridge are rough and uneven, which will result inevitably in moderate errors (of $\sim 10\text{--}15\%$ in total) of the dimensions and hence J_c . On a similar issue, it should be noted that J_c 's determined by transport and magnetization measurements are based on different estimation criteria. The transport J_c is measured directly by a well-defined electrical field or voltage criterion, whereas J_c determined by magnetization depends critically on the underlying assumptions of the critical-state model, which involves different pre-factors related to sample geometry and frequency dependence, for example. Despite these possible sources of error and differences, the J_c values obtained by magnetization and transport measurements in this investigation yield almost similar values.

The transport J_c data obtained in this study are slightly larger than the magnetization J_c data (e.g. 65 kA/cm² vs. 51 kA/cm²), although the difference lies within a realistic and expected range. As stated above, part of the difference is due to the different effective electric field criteria used in the transport and magnetic measurements [20], due possibly in part to the variation in sample size. As a result, the transport data reported here may be considered to be of high quality and constitute proof of principle for this measurement technique. This opens the possibility for future measurements on bulk single-grain (RE)BCO samples of this type, which will significantly extend the depth to which the superconducting

properties of these technologically important materials may be studied for transport current applications, in particular.

4 Conclusions

A GdBCO+Ag single-grain bulk superconductor fabricated via buffer-assisted top-seeded infiltration growth has been used to prepare sample slices for transport measurements and magnetometry. The transition temperature (T_c) and critical current density (J_c) were determined by both characterisation techniques. The resulting T_c values by both approaches were very similar: ~ 93.5 K by magnetometry and 93.7 K by transport. J_c^{sf} at 77 K was ~ 51 kA/cm² via magnetometry and ~ 65 kA/cm² via transport measurements. Despite a 20% variation, these values are relatively similar given the well-known inherent differences between these two measurement techniques. These results indicate that, after a careful preparation of the samples, transport measurements can be performed successfully and reliably on bulk (RE)BCO specimens with a commercial PPMS with modest currents of up to 2 A. This opens the possibility for future measurements for more in-depth electromagnetic investigations of bulk, single-grain (RE)BCO superconductors to gain a deeper understanding of their superconducting properties and their relation to the sample microstructure.

Acknowledgements The authors acknowledge the support received in the form of research grants funded by EPSRC (EP/T014679/1). Data supporting this study are included within the article.

Funding Open access funding provided by University of Geneva.

Data availability All relevant data are included in the paper. Raw data are available from the corresponding authors upon request.

Declarations

Conflict of interest The authors declare no conflict of interest.

Open Access This article is licensed under a Creative Commons Attribution 4.0 International License, which permits use, sharing, adaptation, distribution and reproduction in any medium or format, as long as you give appropriate credit to the original author(s) and the source, provide a link to the Creative Commons licence, and indicate if changes were made. The images or other third party material in this article are included in the article's Creative Commons licence, unless indicated otherwise in a credit line to the material. If material is not included in the article's Creative Commons licence and your intended use is not permitted by statutory regulation or exceeds the permitted use, you will need to obtain permission directly from the copyright holder. To view a copy of this licence, visit <http://creativecommons.org/licenses/by/4.0/>.

References

1. J.H. Durrell, M.D. Ainslie, D. Zhou, P. Vanderbemden, T. Bradshaw, S. Speller, M. Filipenko, D.A. Cardwell, Bulk superconductors: a roadmap to applications. *Sci. Technol.* **31**, 103501 (2018). <https://doi.org/10.1088/1361-6668/aad7ce>
2. D.K. Namburi, Y.H. Shi, D.A. Cardwell, The processing and properties of bulk (RE)BCO high temperature superconductors: current status and future perspectives. *Supercond. Sci. Technol.* **34**, 053002 (2021). <https://doi.org/10.1088/1361-6668/abde88>
3. Y. Zhu, Y. Mu, L. Zeng, M. Wang, X. Yao, Progress in buffer-supported seeding architectures for reliable epitaxial growth of REBa₂Cu₃O_{7- δ} bulk cryomagnets with superior properties *Cryst. Growth Des.* **20**, 7533–7549 (2020). <https://doi.org/10.1021/acs.cgd.0c01131>
4. M. Murakami, *Melt processed high temperature superconductors* (World Scientific Publishing, Singapore, 1999)
5. G. Krabbes, G. Fuchs, W.-R. Canders, H. May, R. Palka, *High temperature superconductor bulk materials: fundamentals – processing – properties control – application aspects* (Wiley, 2006). <https://doi.org/10.1002/3527608044>
6. D.X. Chen, R.B. Goldfarb, Magnetic susceptibility of sintered and powdered Y-Ba-Cu-O. *J. Appl. Phys.* **63**, 980–983 (1988). <https://doi.org/10.1063/1.340050>
7. J.P. Rush, C.J. May-Miller, K.G.B. Palmer, N.A. Rutter, A.R. Dennis, Y.-H. Shi, D.A. Cardwell, J.H. Durrell, Transport J_c in bulk superconductors: a practical approach? *IEEE Trans. Appl. Supercond.* **26**, 6800904 (2016). <https://doi.org/10.1109/TASC.2016.2537647>
8. D.K. Namburi, Y.H. Shi, W. Zhai, A.R. Dennis, J.H. Durrell, D.A. Cardwell, Buffer pellets for high-yield, top-seeded melt growth of large grain Y-Ba-Cu-O superconductors. *Cryst. Growth Des.* **15**, 1472–1480 (2015). <https://doi.org/10.1021/cg501813y>
9. T.S. Kikegawa, H. Sasaki, H. Tada, T. Kudo, H. Kikuchi, K. Konno, M. Muralidhar, M. Murakami, K. Noto, S. Awaji, K. Watanabe, Measurement of critical current for bulk superconductors by transport method. *Physica C* **426–431**, 649–653 (2005). <https://doi.org/10.1016/j.physc.2005.02.099>
10. E.S. Reddy, T. Rajasekharan, Fabrication of textured REBa₂Cu₃O₇/RE₂BaCuO₅ (RE=Y, Gd) composites by infiltration and growth of RE₂BaCuO₅ pre-forms by liquid phases. *Supercond. Sci. Technol.* **11**, 523–534 (1998). <https://doi.org/10.1088/0953-2048/11/5/014>
11. R. Cloots, T. Koutzarova, J.-P. Mathieu, M. Ausloos, From RE-211 to RE-123. How to control the final microstructure of superconducting single-domains. *Supercond. Sci. Technol.* **18**, R9–23 (2005). <https://doi.org/10.1088/0953-2048/18/3/R01>
12. D. Zhou, S. Hara, B. Li, K. Xu, J. Noudem, M. Izumi, Significant improvement of trapped flux in bulk Gd-Ba-Cu-O grains fabricated by a modified top-seeded melt growth process. *Supercond. Sci. Technol.* **26**, 015003 (2013). <https://doi.org/10.1088/0953-2048/26/1/015003>
13. D.K. Namburi, Y.H. Shi, K.G. Palmer, A.R. Dennis, J.H. Durrell, D.A. Cardwell, An improved top seeded infiltration growth method for the fabrication of Y-Ba-Cu-O bulk superconductors. *J. European. Ceram. Soc.* **36**, 615–624 (2016). <https://doi.org/10.1016/j.jeurceramsoc.2015.09.036>
14. D. Das, M. Muralidhar, M.S.R. Rao, M. Murakami, Top-seeded infiltration growth of (Y, Gd)Ba₂Cu₃O_y bulk superconductors with high critical current densities. *Supercond. Sci. Technol.* **30**, 105015 (2017). <https://doi.org/10.1088/1361-6668/aa83da>
15. L. Vojtkova, P. Diko, D. Volochová, V. Kavecanský, V. Antal, S. Piovarci, Top-seeded infiltration growth and structure of YBCO bulk superconductors. *IEEE Trans. Appl. Supercond.* **26**, 7200704 (2016). <https://doi.org/10.1109/TASC.2016.2542275>
16. G.-Z. Li, D.-J. Li, X.-Y. Deng, J.-H. Deng, W.-M. Yang, Infiltration growth and crystallization characterization of single grain Y-Ba-Cu-O bulk superconductors. *Cryst. Growth Des.* **13**, 1246–1251 (2013). <https://doi.org/10.1021/cg301703t>
17. T. Naito, T. Sasaki, H. Fujishiro, Trapped magnetic field and vortex pinning properties of MgB₂ superconducting bulk fabricated by a capsule method. *Supercond. Sci. Technol.* **25**, 095012 (2012). <https://doi.org/10.1088/0953-2048/25/9/095012>
18. P. Cayado, M. Erbe, S. Kauffmann-Weiss, C. Bühler, A. Jung, J. Hänisch, B. Holzapfel, Large critical current densities and pinning forces in CSD-grown superconducting GdBa₂Cu₃O_{7- x} - BaHfO₃ nanocomposite films. *Supercond. Sci. Technol.* **30**, 094007 (2017). <https://doi.org/10.1088/1361-6668/aa7e47>
19. P. Cayado, H. Rijckaert, E. Bruneel et al., Importance of the pyrolysis for microstructure and superconducting properties of CSD-grown GdBa₂Cu₃O_{7- x} -HfO₂ nanocomposite films by the ex-situ approach. *Sci Rep* **10**, 19469 (2020). <https://doi.org/10.1038/s41598-020-75587-4>
20. A.V. Pan, I.A. Golovchanskiy, S.A. Fedoseev, Critical current density: Measurements vs reality. *Europhys. Lett.* **103**, 17006 (2013). <https://doi.org/10.1209/0295-5075/103/17006>

Publisher's Note Springer Nature remains neutral with regard to jurisdictional claims in published maps and institutional affiliations.